

Climatology of Upper-Tropospheric Relative Humidity from the Atmospheric Infrared Sounder and Implications for Climate

ANDREW GETTELMAN AND WILLIAM D. COLLINS

National Center for Atmospheric Research, Boulder, Colorado*

ERIC J. FETZER, ANNMARIE ELDERING, AND FREDRICK W. IRION

NASA Jet Propulsion Laboratory, California Institute of Technology, Pasadena, California

PHILLIP B. DUFFY AND GOVINDASAMY BALA

Lawrence Livermore National Laboratory, Livermore, California

(Manuscript received 9 August 2005, in final form 31 March 2006)

ABSTRACT

Recently available satellite observations from the Atmospheric Infrared Sounder (AIRS) are used to calculate relative humidity in the troposphere. The observations illustrate many scales of variability in the atmosphere from the seasonal overturning Hadley–Walker circulation to high-frequency transient variability associated with baroclinic storms with high vertical resolution. The Asian monsoon circulation has a strong impact on upper-tropospheric humidity, with large humidity gradients to the west of the monsoon. The vertical structure of humidity is generally bimodal, with high humidity in the upper and lower troposphere, and a dry middle troposphere. The highest variances in humidity are seen around the midlatitude tropopause. AIRS data are compared to a simulation from a state-of-the-art climate model. The model does a good job of reproducing the mean humidity distribution but is slightly moister than the observations in the middle and upper troposphere. The model has difficulty reproducing many scales of observed variability, particularly in the Tropics. Differences in humidity imply global differences in the top of atmosphere fluxes of $\sim 1 \text{ W m}^{-2}$.

1. Introduction

Water vapor is the principal greenhouse gas in the atmosphere. Changes to absorption of radiation by water vapor are expected to contribute significantly to changes in radiative forcing, known as the water vapor feedback (Hartmann and Michelsen 2002). Water vapor in the upper troposphere, while insignificant by total mass of column water vapor, can have significant effects on climate, through the formation of clouds (longwave cloud forcing) or by direct absorption of ra-

diation. Udelhofen and Hartmann (1995) estimated with a radiative transfer model that a 10% increase in upper-tropospheric humidity (UTH) could contribute as much as 1.4 W m^{-2} of direct radiative forcing. UTH is especially critical in the dry subtropics (Hartmann and Larson 2002) where the radiative forcing of humidity at upper levels above a dry troposphere can be even larger (Jensen et al. 2000).

Understanding the distribution and variability of UTH is critical for understanding and simulating current climate and future climate change. General circulation models (GCMs) must represent the vertical and horizontal structure of humidity properly, or else the resulting biases in radiative heating may impact the circulation. Unfortunately, UTH is difficult to measure, and few comprehensive datasets exist with appropriate vertical resolution and temporal coverage. Radiosonde humidity sensors are unreliable in the upper troposphere (Elliot and Gaffen 1991; Miloshevich et al. 2006) and spotty coverage can lead to biases in regions not

* The National Center for Atmospheric Research is sponsored by the National Science Foundation.

Corresponding author address: Andrew Gettelman, National Center for Atmospheric Research, 1850 Table Mesa Drive, Boulder, CO 80305.
E-mail: andrew@ucar.edu

well covered by radiosondes, especially in the Tropics and subtropics (Soden and Lazante 1996). Several previous efforts have been made to use satellite datasets to understand UTH. Rind et al. (1993) used data from the Stratospheric Aerosol and Gas Experiment II (SAGEII) to develop a climatology of specific humidity down to 300 hPa. Soden and Bretherton (1994) used 6.7- μm brightness temperature from a single Geostationary Operational Environmental Satellite (GOES) to estimate UTH with a broad (3–5 km) thick weighting function, and Soden and Fu (1995) extended this globally. This method was refined and extended by Jackson and Bates (2001). Read et al. (1995, 2001) used data from the Microwave Limb Sounder (MLS) on the *Upper Atmosphere Research Satellite* (UARS) to develop a climatology of relative humidity over ice (RH_i) at 215 and 147 hPa with 200-km horizontal and 3-km vertical resolution.

In this work we present a new dataset of global measurements of relative humidity (RH) throughout the troposphere from the Atmospheric Infrared Sounder (AIRS) on the NASA *Aqua* satellite. What AIRS adds to the existing observations is high vertical resolution combined with global daily coverage. AIRS is also the first of a new class of high spectral resolution satellite sensors, which will be used to monitor weather and climate for the next 20 years. We use this data to better understand variability of humidity in the upper troposphere on various time and space scales. We compare this variability to state-of-the-art climate model simulations. In a companion paper (Gettelman et al. 2006a), we use the data to focus on those regions that are supersaturated with respect to ice.

2. Data description

AIRS on *Aqua* is in a sun-synchronous polar orbit with equatorial crossings at ~ 1330 and ~ 0130 local time. The AIRS instrument suite is a nadir-scanning sounder with combined infrared and microwave retrievals (Aumann et al. 2003). The ~ 2000 independent channels of AIRS permit retrieval of an entire profile in the presence of up to 70% cloud fraction. AIRS cloud fraction is defined as the product of cloud coverage and infrared emissivity. We use AIRS level-2 data retrievals (version 3.0), described by Fetzer et al. (2003; see also <http://www-airis.jpl.nasa.gov/>). AIRS uses a regression-based retrieval, and the process optimizes the fit to a subset of the AIRS channels (147 for temperature, 66 for H₂O, and 23 for O₃). AIRS retrievals use overlapping trapezoidal perturbation functions with widths in the upper troposphere/lower stratosphere (UT/LS) of

~ 2 km for temperature and 1–3 km for H₂O. This yields an effective vertical resolution of slightly less than these values (Susskind et al. 2003). Horizontal resolution is approximately ~ 45 km, and there are on the order of 300 000 AIRS profiles per day. AIRS standard retrieved products are archived on 28 levels from the surface to the mesosphere.

We use standard level-2 retrieved profiles. Only data for which the infrared retrieval is successfully completed are used. Water vapor (q) and temperature retrievals are used to derive relative humidity (RH = $q/q_s \times 100$ in percent) for each profile. We further restrict the calculation of RH to regions where water vapor is greater than 10 ppmv, the nominal reported instrument sensitivity. The saturation vapor mixing ratio q_s is calculated using the formulation of Goff and Gratch (1946) over water for temperatures >273 K (0°C) and over ice for temperatures <253 K (–20°C), with a linear combination of the two between them. This formulation is identical to that in the Community Atmosphere Model version 3 (CAM3) described by Collins et al. (2006) and facilitates comparisons. At temperatures ~ 200 K and above, uncertainties in q_s are 1%–2% (Murphy and Koop 2005).

Profiles of relative humidity at ~ 45 -km resolution are binned into a 1° by 1° latitude–longitude grid. Longitude bins are held constant at 111 km (so that more profiles are found in each bin near the poles). Since the version 3 retrievals provide a column water vapor, (\bar{q}), between two pressure levels and temperature on the level edges, we construct a column saturation vapor pressure (\bar{q}_s) by numerically integrating the saturation vapor pressure assuming temperature in the layer is linear between the two edges. We have conducted a detailed sensitivity test of the method of calculating relative humidity, and the results are not highly sensitive to the method chosen. Following the AIRS convention, pressures here refer to the bottom of the layer.

A sample of the resulting data is illustrated in Fig. 1 showing temperature, water vapor, and RH for 6 January 2005 at 250 hPa (representing the layer from 250–200 hPa). We choose this level for comparison as it shows variability in the Tropics as well as in the extratropics. The layer at 250-hPa is near the height of the extratropical tropopause (the red line in Fig. 1 is the tropopause at 225 hPa, the layer midpoint), diagnosed from National Centers for Environmental Prediction–National Center for Atmospheric Research (NCEP–NCAR) reanalysis data. A tropopause derived from AIRS temperature profiles looks very similar, but missing data points make presentation difficult. AIRS data coverage in Fig. 1 is typical for one day, with no data

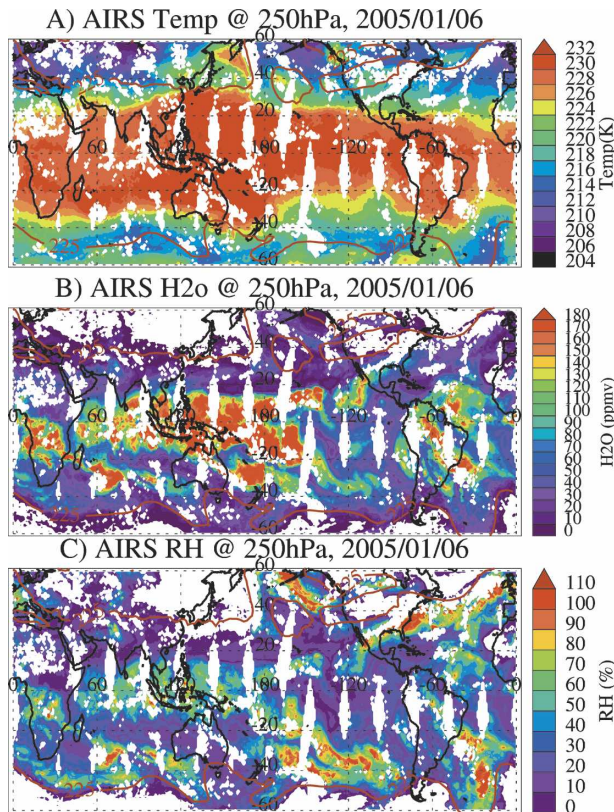


FIG. 1. Gridded AIRS data at 250 hPa for 6 Jan 2005: (a) Temperature (K), (b) water vapor (ppmv), and (c) relative humidity (%). Solid line is NCEP-NCAR reanalysis tropopause pressure on this day.

when cloud coverage is higher than about 70% in all nine 15-km pixels, and gaps in coverage in the Tropics where the orbit tracks do not overlap. These gaps progress on an 8-day repeat cycle.

Temperatures at this level are warmer in the tropical troposphere than in the extratropical lower stratosphere (Fig. 1a). Water vapor is higher in the troposphere in the Tropics (Fig. 1b) with extreme variations regionally from ~ 200 ppmv in active convective regions of the western Pacific, Africa, and South America to 20–50 ppmv in dry regions of the eastern Pacific. Water vapor data have a different quality threshold than temperature data, so the missing data are different. The extratropics is drier, and much of this region is in the stratosphere. Relative humidity is different (Fig. 1c). Note that RH data is missing if either water vapor (Fig. 1b) or temperature (Fig. 1a) data are missing or do not meet the quality criteria. The convective areas of the Tropics have RH of 60%–90%, and the dry eastern Pacific and subtropics have humidities of less than 30%. The extratropics have high variability, ranging from nearly zero RH (representing stratospheric air) to

90%–100% in midlatitude storm systems (tropospheric air, warm conveyor belts), which are beneath the tropopause. Note how RH is high in the troposphere and low in the stratosphere, which need not be zonal but can extend up to high latitudes, as in the North Pacific to 60°N and the South Atlantic to 60°S. We investigate the statistics of this variability further below.

Validation of AIRS water vapor, temperature, and relative humidity data is ongoing with balloons and aircraft data. Much of this validation is confined to or focused on the lower troposphere for separate temperature and water vapor retrievals. Tobin et al. (2006) note that AIRS meets or exceeds the design specification of 1-K temperature and 20% water vapor accuracy for the tropical upper troposphere over ocean, with rms differences from radiosondes slightly higher than this in the UT over land based on dedicated validation sites. Using the globally available radiosonde record, Divakarla et al. (2006) find similar results with potential temperature biases relative to radiosondes of $\sim +0.5$ K at 600 hPa and ~ -0.5 K at 300 hPa, possibly due to temporal variations in carbon dioxide absorption slightly biasing the retrieval. Divakarla et al. found no biases in the AIRS water vapor retrieval. These results generally validate the AIRS retrievals of temperature and humidity to within the design specifications.

Since our focus is on the upper troposphere, of most relevance to this study is the work of Gettelman et al. (2004), who compared AIRS profiles collocated to in situ aircraft data in the UT/LS region and found that AIRS temperatures matched aircraft temperatures, without bias, and with a standard deviation (σ) of 1.5 K. Water vapor below 150 hPa is also well reproduced, with a standard deviation of 20%. Relative humidity at 250 hPa and below is also unbiased, with $\sigma = 9\%$. AIRS retrieves for cloud fractions < 0.7 . Based on analyses by Soden and Fu (1995) comparing Television Infrared Observation Satellite (TIROS) Operational Vertical Sounder (TOVS) UTH with radiosondes, it is estimated that the dry bias introduced is of the order of 4% RH. The bias is a function of RH (since high RH is found in regions of cloudiness) and is larger for more humid regions.

Also relevant is comparison of AIRS with dedicated radiosondes over the cold Antarctic ice sheet. AIRS retrievals of relative humidity are within the uncertainty of in situ observations based on dedicated radiosondes launched over Dome C Station in Antarctica at -75°S , 123°E (Gettelman et al. 2006b). This illustrates that AIRS RH retrievals are of high quality, even for difficult conditions in the upper troposphere, and even over elevated ice sheets. In this work we limit our analyses to regions equatorward of 70° latitude.

3. Climatology

In this section we describe the climatological distribution of RH observed from AIRS in the upper and lower troposphere, along with the vertical structure of RH in key regions. Then we describe RH variability at individual points and its vertical structure, as well as global variations on time scales from daily to seasonal.

The seasonal evolution of RH at 250 hPa from AIRS is illustrated in Fig. 2. This level is in the upper troposphere, but still within the range of validated AIRS data, and is a level with little obvious temperature bias (Divakarla et al. 2006). The climatological picture from AIRS data on a seasonal basis (Fig. 2) is similar to that observed from other instruments (Rind et al. 1993; Read et al. 1995; Bates and Jackson 2001). High relative humidities are observed in the tropical upper troposphere in convective regions in the Tropics. Peak RH migrates from south of the equator in December–February (Fig. 2a) to north of the equator in June–August (Fig. 2c). Lower humidities are found in the subtropical winter hemisphere, evidence of the overturning Hadley–Walker circulation. The equatorial eastern Pacific is the driest region of the Tropics throughout the year. In the upper troposphere, the Asian summer monsoon and North American monsoon dominate in boreal summer (June–August, Fig. 2c). Polar latitudes at this pressure are often in the stratosphere (poleward of the tropopause indicated in Fig. 2) and have very low humidities throughout the year.

Very low RH is found equatorward of the tropopause in the north-central Pacific in December–February (Fig. 2a), over Central Asia and the Middle East in June–August (Fig. 2c), as well as to a lesser extent in all other seasons, and over the south Indian Ocean and Australia from June–November (Figs. 2c,d). Low RH in the central Pacific is described by Waugh (2005). An examination of individual days from the data record indicates that these low RH regions mostly do not meet the quality threshold for RH ($q > 10$ ppmv), except on a few days per month. This is especially true for the region over the Middle East, just west of the Asian monsoon in June–August (Fig. 2c). These observations are at the edge of the AIRS data range, but they are corroborated by other observations of upper-tropospheric water vapor and humidity. Read et al. (1995) observed low water vapor at 215 hPa over the Middle East and southern Indian Ocean extending all the way to Africa from the MLS instrument during June–August (similar to Fig. 2c). Read et al. indicate low humidities over the North Pacific and East Asia from December to February, similar to Fig. 2a. Rind et al. (1993) also observed low specific humidity from SAGE

at 300 hPa, in the North Pacific in January (as in Fig. 2a) and over the Middle East and South Indian Ocean in July (as in Fig. 2c).

Humidity is very low over the Middle East in June–August west of the Asian monsoon because temperatures at 250 hPa are still relatively warm, but the air is very dry. It appears that the region is isolated from the moisture of the Asian monsoon complex, despite being embedded in the monsoon anticyclone at these levels. Some of the dynamics of this region and interactions with convection are illustrated in more detail by Randel and Park (2006).

The lower troposphere (Fig. 3) is different from 250 hPa. Most notable for climate are the extreme dry regions in the winter subtropics (Northern Hemisphere in December–February in Fig. 3a and Southern Hemisphere in June–November in Figs. 3c and 3d). This is especially true of the subtropical eastern Pacific and Atlantic. Humidity is high in the intertropical convergence zone. The ITCZ migrates throughout the year following the sun (maximizing in the Southern Hemisphere). In the eastern Pacific and Atlantic, the RH maximum stays north of the equator throughout the whole year. Convective regions over South America, the western Pacific, and Africa persist throughout the year and migrate with the ITCZ. Along with convection over Africa, the Asian summer monsoon surrounding the Bay of Bengal has a large region of high RH in the lower troposphere in June–August (Fig. 3c). Higher humidities are also seen in polar regions in winter, due likely to extremely cold temperatures.

The real power of AIRS data lies in its vertical resolution in the troposphere. Figure 4a illustrates a vertical cross section along 45° latitude of the seasonal mean AIRS RH for December–February. As in Fig. 2a, there are regions of high humidity in the upper troposphere, right up to the tropopause. These regions follow the tropopause structure and seem to peak over the North Pacific, North Atlantic, and north Central Asia extending down to 400 hPa. A similar plot for temperature (not shown) indicates that this is near the 235-K temperature contour, above which we expect ice processes to dominate. There are also high humidities confined below 700 hPa over oceans. The midtroposphere is relatively dry, even at high latitudes in winter, with humidities from 20% to 40% in a layer from 800 to 500 hPa (2 to 5 km). The North Atlantic has high humidity above and below this layer with a minimum in the free troposphere. Low RH is seen near the surface over the high plateaus of Mongolia and the Rocky Mountains of North America. There may be anomalies in AIRS retrievals caused by high topography.

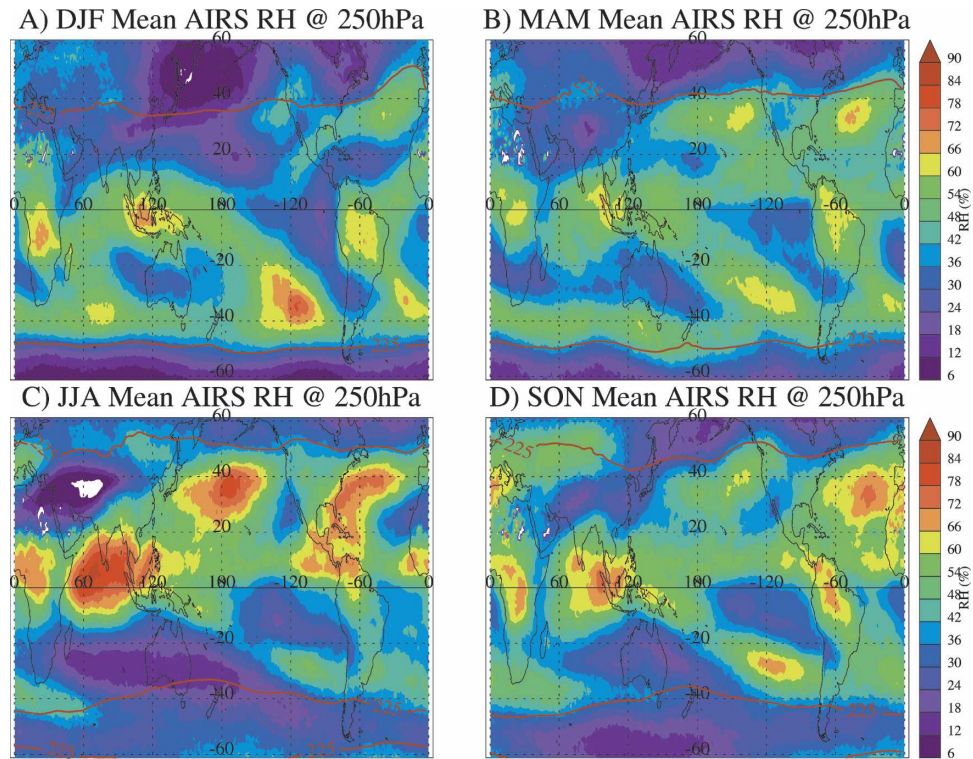


FIG. 2. Seasonal mean AIRS relative humidity (%) at 250 hPa for (a) Dec–Feb, (b) Mar–May, (c) Jun–Aug, and (d) Sep–Nov. Solid line indicates the AIRS tropopause at 225 hPa.

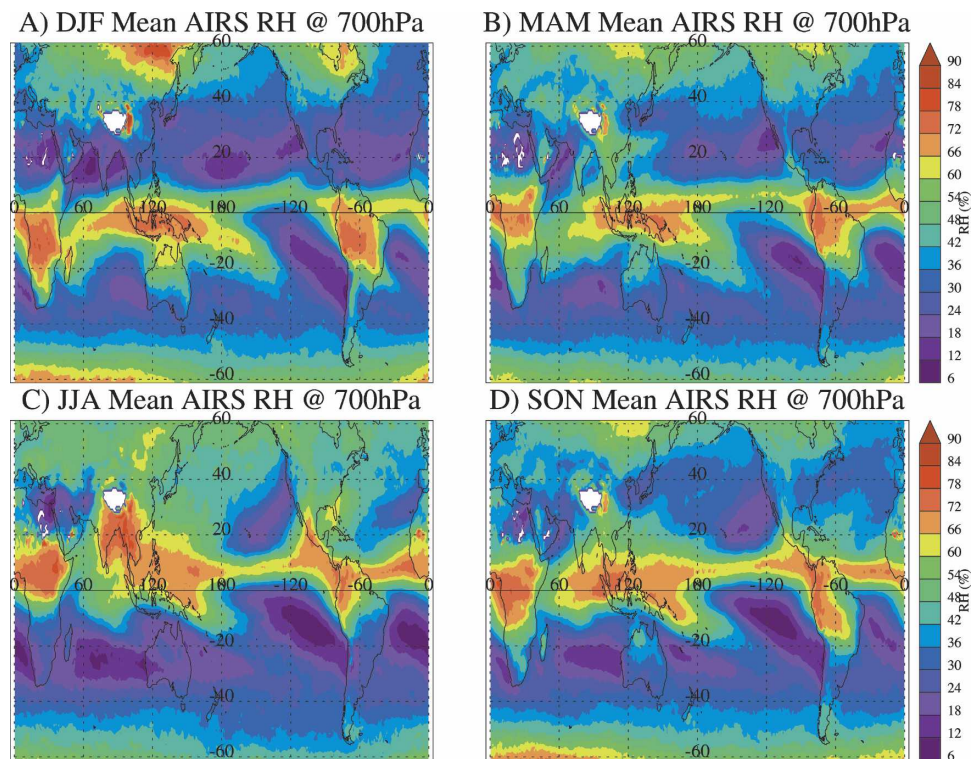


FIG. 3. Seasonal mean AIRS relative humidity (%) at 700 hPa for (a) Dec–Feb, (b) Mar–May, (c) Jun–Aug, and (d) Sep–Nov.

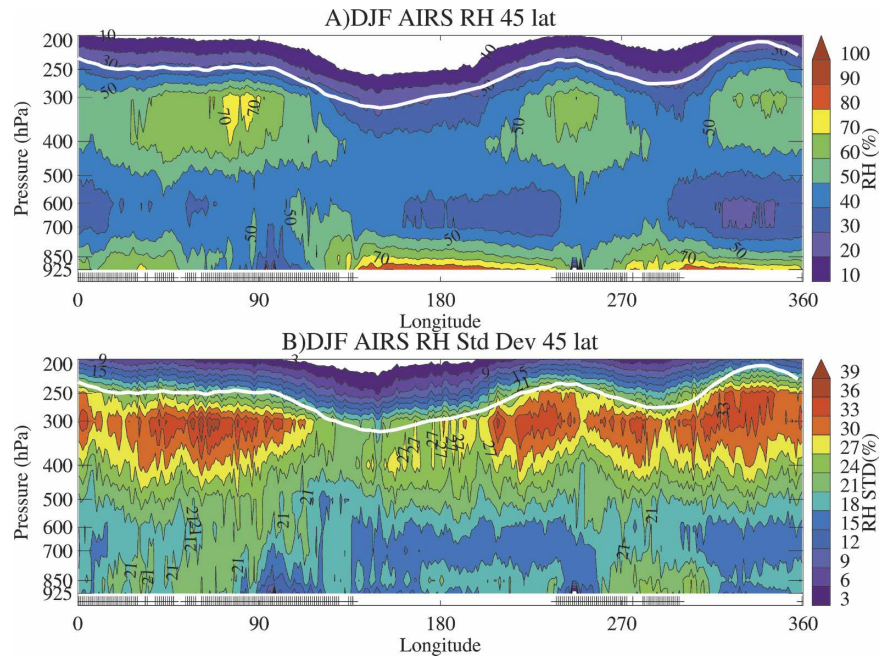


FIG. 4. Longitude vs pressure cross sections of Dec–Feb seasonal mean AIRS: (a) RH (%) and (b) RH standard deviation at 45°N latitude. Crosses indicate landmasses at this latitude; solid white line is the NCEP–NCAR reanalysis seasonal mean tropopause.

The Tropics has a slightly different vertical structure, illustrated in Fig. 5a for the summer season (December–February). As at high latitudes, at 10°S there is a broad minimum in RH in the middle troposphere but

big regional differences, with a very moist lower troposphere over all regions except the tropical eastern Pacific and Atlantic. Over these regions of subsidence, humidities throughout the troposphere from 850 to 300 hPa

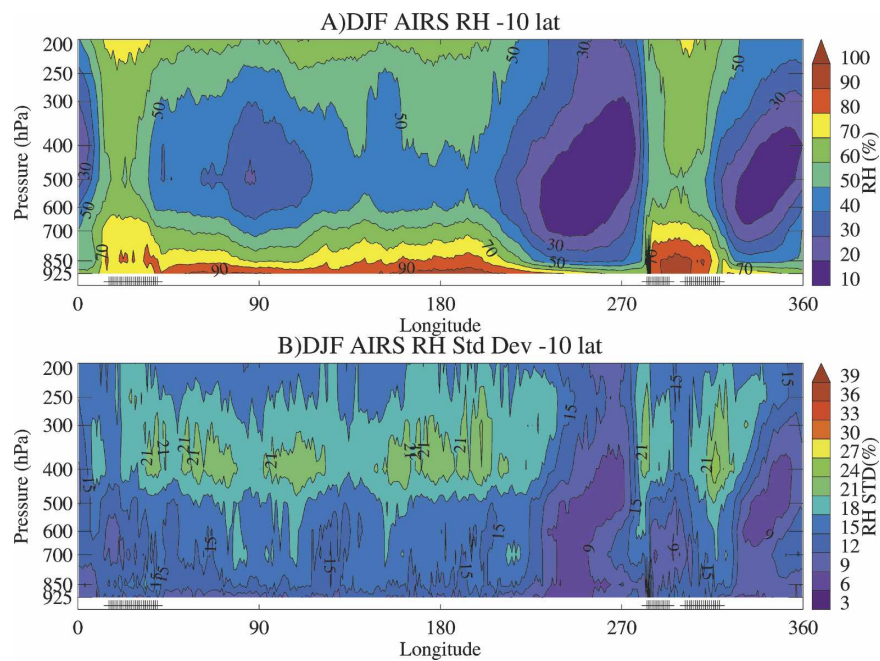


FIG. 5. As in Fig. 4 but for Dec–Feb at 10°S latitude.

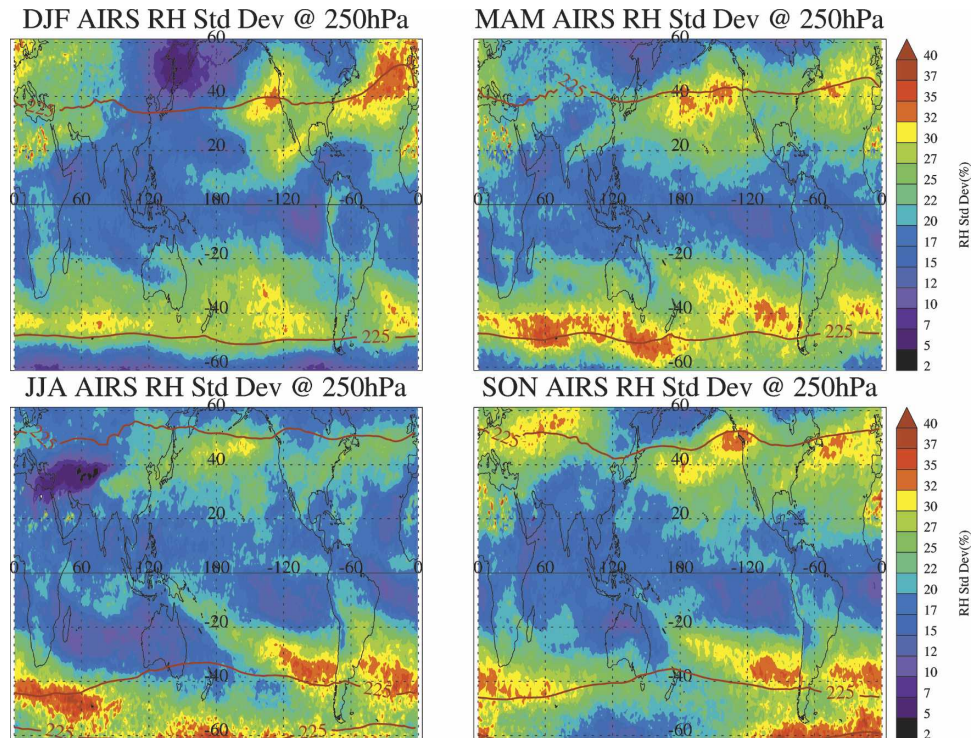


FIG. 6. As in Fig. 2 but for seasonal mean standard deviation of AIRS relative humidity (%).

are below 20%. High humidities are found in deep layers over the tropical convective regions of South America, Africa, and the western Pacific. The upper troposphere also has high RH over most of the Tropics except for the subsidence regions in the tropical east Pacific and Atlantic. Highest RH (over 70%) is found over the land convective regions of South America and Africa. A similar picture of low RH in subsidence regions of the eastern ocean basins and high RH in convective regions exists in the Northern Hemisphere during summer (not shown).

AIRS data can also provide high temporal resolution data. Figure 6 illustrates the standard deviation of daily RH (σ_{RH}) on a seasonal basis in the upper troposphere. The data is based on 2.5 years of daily data, so each season has a minimum of 180 days of data. The standard deviation, σ_{RH} , in the Tropics is $\sim 20\%$. Wintertime storm tracks in each hemisphere show the highest σ_{RH} (30% or higher), which is linked to regions right near the tropopause (thick line in Fig. 6). The position of the mean tropopause neatly bounds the region of high RH variability in the wintertime North Atlantic in Fig. 6a, which is also seen in the single day plotted in Fig. 1c.

Variability maxima in Fig. 6 are similar to the maxima in Lagrangian warm conveyor belts found by Eckhardt et al. (2004). Differences are largest in the

North Pacific storm track where at 250 hPa AIRS sees maxima in late winter and spring (March–May, Fig. 6b), though this could be due to interannual variability of the storm tracks. High variability regions are similar throughout the year and seem to peak just equatorward of the mean tropopause location for this layer (250–200 hPa). This is to be expected in the upper troposphere and lower stratosphere, as humidity associated with uplifted air in baroclinic storms and warm conveyor belts alternates with very dry stratospheric air. The Southern Hemisphere tropopause region has higher σ_{RH} than the Northern Hemisphere in Fig. 6, and high σ_{RH} is seen at almost all longitudes. This might simply be due to the position of the tropopause, which is closer to this layer all the way to 60°S latitude in winter (Fig. 6c).

The vertical structure of variability in the storm track region is highlighted in Fig. 4b for Northern Hemisphere winter. High variance is found corresponding to the regions of a higher averaged tropopause altitude and high mean RH (Fig. 4a). Variability is also high near the surface over land (Asia and North America) and, as expected, is lower over the oceans. Interestingly, the variability in the Tropics is slightly different (Fig. 5b) than in middle latitudes (Fig. 4b). At 10°S in December–February, typical of the Tropics, variability is low over the surface, even in convective regions, and peaks in the middle troposphere at about 400 hPa (7

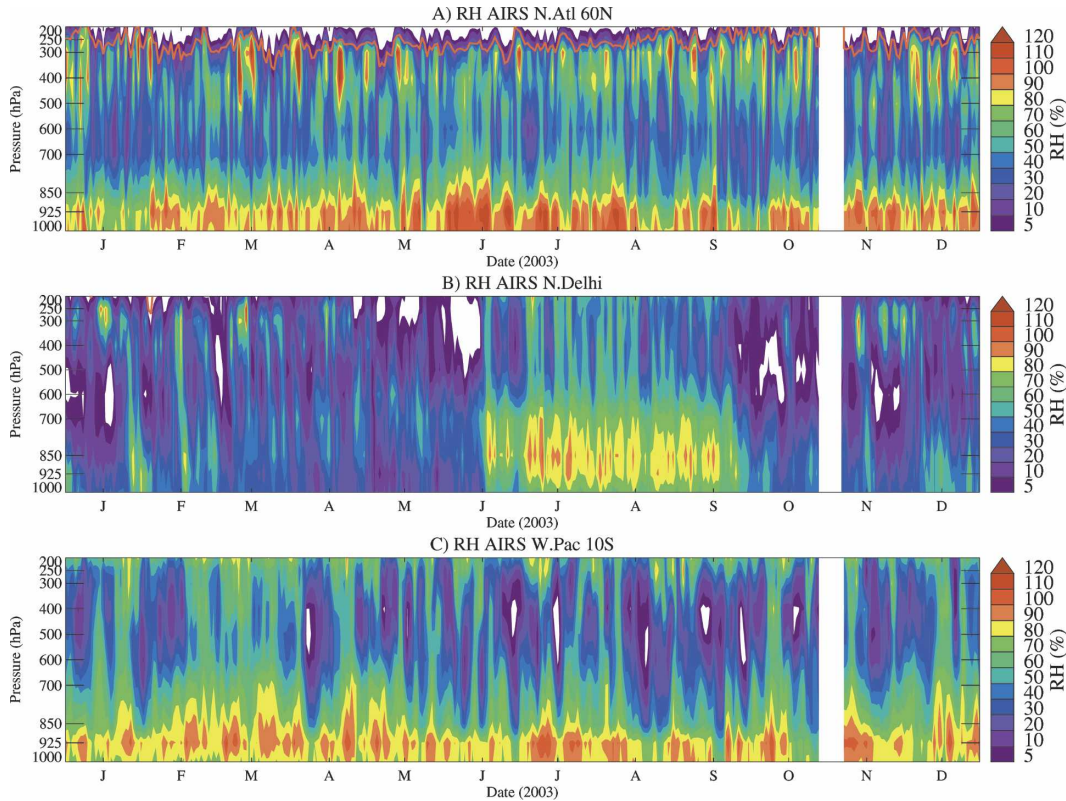


FIG. 7. Time-height plot of daily AIRS RH (%) for 2003 as a function of pressure for a $5^{\circ} \times 5^{\circ}$ region over (a) the North Atlantic (60°N , 330°E), (b) New Delhi, India (28°N , 77°E), and (c) the western Pacific (10°S , 150°E). Red line indicates the daily NCEP-NCAR reanalysis tropopause.

km). Midtropospheric variability is slightly lower in convective regions (over South America and Africa) and higher at the edge of those regions. This variability might be related to midtropospheric convective detrainment, or convective effects on local subsidence.

The global coverage and temporal frequency enable AIRS data to be used for detailed investigations of daily variability. The vertical structure of daily variability is illustrated in Fig. 7a for a $5^{\circ} \times 5^{\circ}$ region of the North Atlantic during 2003. Variations in RH at upper levels are tightly correlated with the tropopause, which is estimated from an independent data source (the NCEP-NCAR reanalysis) in Fig. 7a. Synoptic variability dominates, with variations in a few days from near saturation (90%–110% RH over ice at these altitudes) to values of 20%–40% RH in eastward propagating storm systems (evident if all longitudes are sampled). Highest humidities are seen from August through October. Midtropospheric (500–800 hPa) dryness is a persistent feature. The lower troposphere here is near saturation most of the year over the ocean. The vertical structure and relationship with tropopause height is one of many phenomena in the AIRS climatology warrant-

ing further investigation. Southern Hemisphere mid-latitudes (not shown) appear to be similar, with slightly lower variability consistent with Fig. 6.

Figure 8 is a Hovmöller plot for a single year of AIRS data (2003) averaged over the subtropical Northern Hemisphere from 10° to 30°N . Bilinear interpolation has been used on each day of data for input to Fig. 8. The subtropics are a critical region for the atmosphere radiating energy to space, and the efficiency of radiation in this region is important for understanding the atmospheric heat engine (Hartmann and Larson 2002).

In the upper troposphere (Fig. 8), the winter hemisphere is extremely dry in the subtropics with RH values below 20%. Some of this air may be in the stratosphere. Variability is high and maximizes in the central and eastern Pacific with subtropical intrusions bringing dry air masses from the stratosphere. As described by Waugh (2005), these low humidity events coincide with high potential vorticity and high ozone, indicating a stratospheric influence. In boreal summer, the influence of the Asian monsoon over the Indian Ocean and the ITCZ from the Pacific to Atlantic is dominant. The dry region to the west of the Asian monsoon is evident

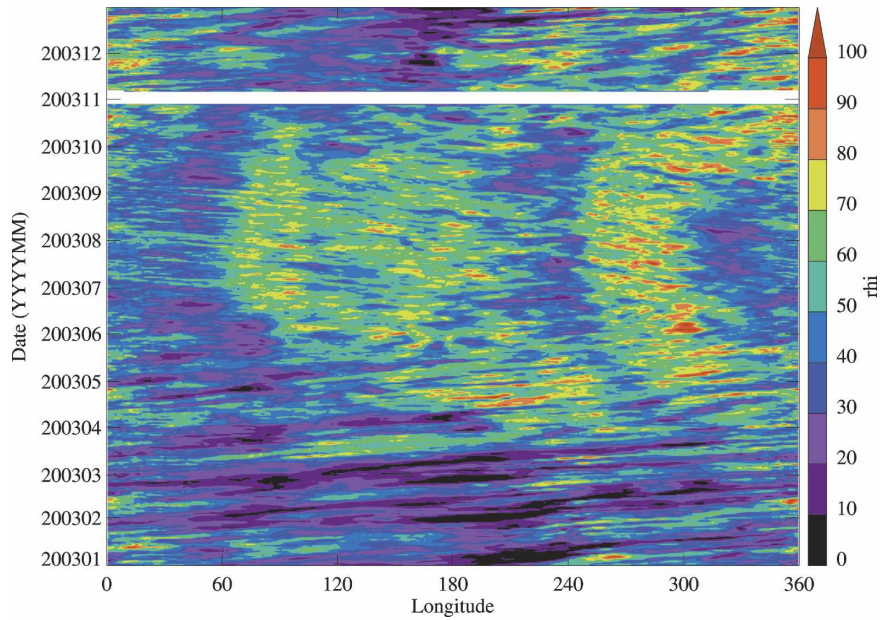


FIG. 8. Hovmöller plot of daily AIRS RH (%) at 250 hPa averaged over 10° – 30° N latitude.

in June–August. Note also that the dominant transient features are easterly wave events from the western Pacific and Asian monsoon westward into the Atlantic through the dry region in Fig. 2. It is likely that these events are due to outflow of upper-level moisture from the equatorward branch of the Asian monsoon. The seasonal transitions are fairly well marked, from the

winter time intrusions to the summer monsoon circulations, which then evolve back into winter storm tracks. The Southern Hemisphere (not shown) has a similar structure, with the exception that the Australasian monsoon circulation is not as strong in austral summer and the South Pacific convergence zone in the western and central Pacific is dominant through the austral summer.

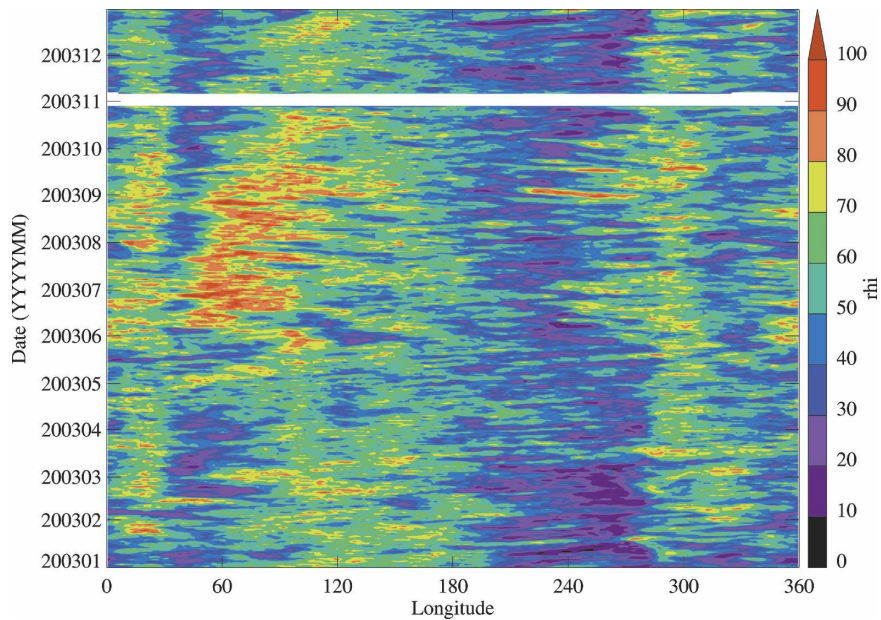


FIG. 9. As in Fig. 8 but averaged over 10° S– 10° N latitude.

Figure 7b illustrates a vertical cross section of daily RH centered over New Delhi, India (28°N , 77°E), for 2003. At this location over land, most of the troposphere is quite dry for most of the year. The dominant feature is the sudden jump to 80%–90% humidity during the South Asian monsoon from July to September from the surface to 700 hPa. Convection also likely explains the hydration of the middle and upper troposphere during the monsoon season in Fig. 7b. Relative humidity at 200–400 hPa goes from 10%–20% in May to 60%–80% in June. AIRS cannot see the uppermost troposphere where monsoon convection detrains. The middle troposphere (700–400 hPa) over central India is extremely dry outside of the monsoon season.

In the Tropics (Fig. 9) the dominant features of the distribution are persistent regions of high humidity over convective regions (Africa, western Pacific, and South America), low humidity over the eastern Pacific, and a large signature of high humidity over the Indian Ocean from June to September, likely associated with the Asian monsoon north of the equator. The vertical structure is illustrated in Fig. 7c for a point in the western Pacific at 10°S (150°E). There is high RH near the surface and increasing RH in the upper troposphere, up to 80% at 200 hPa, with RH still increasing with height. Upper-tropospheric moistening appears to be linked to convection and occurs more in the summer season (December–February). The middle troposphere is relatively dry from 700 to 300 hPa, more so in northern winter. These features are consistent in the same seasons north of the equator. Note that the time scale of the high humidity episodes is longer than at higher latitudes Fig. 7a.

In boreal winter, westerly propagating high humidity maxima with a periodicity of about 2 months are seen (beginning of February at 0° longitude to the latter half of March), representing the Madden–Julian oscillation (MJO). The MJO has been seen in previous analyses of UTH from other sources (Eguchi and Shiotani 2004; Mote et al. 2000). Such maxima are also seen in Fig. 7c during mid-January and late February 2003 (a 30–50-day period). The vertical structure is similar to other convective events, with the whole troposphere moistening.

During the period of the Asian monsoon, easterly waves are seen in the Indian Ocean region in the Tropics, originating in the eastern Indian Ocean (Fig. 9). High RH is also associated with the Australasian monsoon around 120°E longitude from January to April. The eastern Pacific remains dry throughout the year, with the driest air migrating off the coast of South America from June to October as convection moves into the Gulf of Panama at 250° – 270° longitude. High

humidity events that rapidly propagate to the west in the eastern Pacific and Atlantic from June to September are associated with tropical cyclones, and several of these can clearly be seen in the AIRS record.

AIRS provides data coverage from September 2002, so as of late 2005 it is not really possible to look at interannual variability. The record is too short to draw conclusions. We have examined several locations and note simply that AIRS is a repeatable annual cycle with variability from year to year that is less than one standard deviation of the day-to-day variations.

4. Model comparisons

Matching observed profiles of water vapor is an important requirement for simulating the climate system. AIRS provides data at a resolution similar to GCMs used to simulate the climate system. Here we provide comparisons of a climatology of the NCAR CAM3, described by Collins et al. (2006). For comparison we use a simulation at $1^{\circ} \times 1.25^{\circ}$ horizontal resolution and 26 levels in the vertical with surface temperatures taken from observations during 2000–2004. We use daily averaged output for comparison to the satellite data for the year 2003. Our focus is on understanding 1) simulations of mean relative humidity, 2) the variability in those simulations, and 3) the implications for climate of differences between observations and the model. To facilitate comparisons with AIRS IR observations, which are biased toward clear sky scenes, we average only those simulated points with cloud fraction less than 70% in all of these analyses.

a. Simulations of the mean

The monthly mean vertical structure of humidity in several key regions from CAM and AIRS is illustrated in Fig. 10. These profiles show the vertical structure, illustrated in Figs. 4, 5, and 7, with higher RH at lower and upper levels and a midtropospheric minimum. In the tropical western Pacific (Fig. 10a) in January, CAM does a good job of reproducing the relative humidity profile, except it is too moist around 500 hPa. In the subtropical eastern Pacific (Fig. 10b) in July, CAM is generally 10%–20% more moist than AIRS throughout the troposphere, by nearly 50% of the AIRS value. This is also true for other subtropical regions. Note that the differences at upper levels are not significant since both of these datasets have large uncertainties above the tropopause. CAM RH is also higher than AIRS RH above the North Atlantic in January (Fig. 10c), with moderate differences except at around 700 hPa where it appears that the simulation does not sufficiently contain boundary layer humidity near the surface.

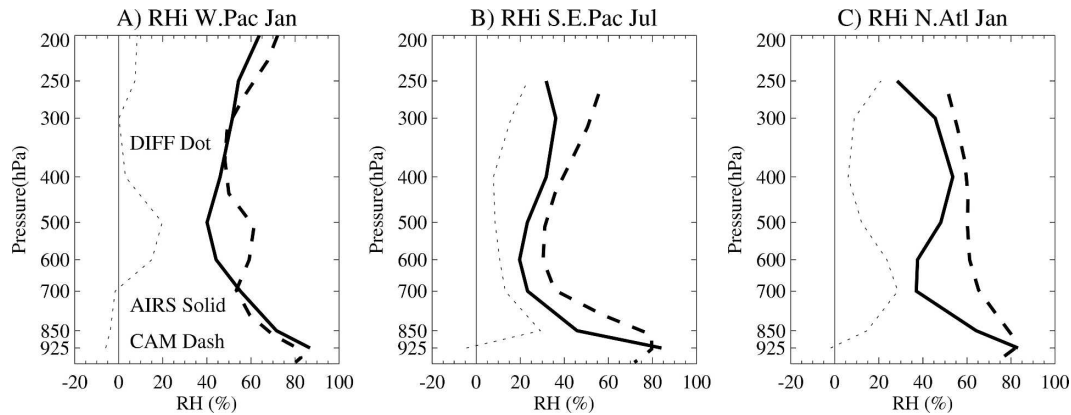


FIG. 10. Monthly mean RH (%) profiles for AIRS (solid), CAM (dashed), and difference (CAM – AIRS) (dotted) at the (a) western Pacific (15°S – 15°N , 120°E – 180°) in Jan, (b) southeastern Pacific (35° – 15°S , 200° – 260°E) in Jul, and (c) North Atlantic (45° – 65°N , 300°E – 360°) in Jan.

To generalize the results in Fig. 10, we first examine maps of simulated RH in the upper (~ 250 hPa) and lower (~ 700 hPa) troposphere. We then quantitatively examine zonal mean differences. Figure 11 illustrates the model RH at 226 hPa for 2003. This level is approximately the middle of the AIRS 250-hPa layer illustrated in Fig. 2. To facilitate comparison with AIRS observations, seasonal means are for points with cloud fraction less than 70%. Relative humidity is generally higher than in the observations. Some of this may be due to a dry bias in the AIRS data (even after screening for cloudiness). Most of the major features are reproduced however. Maxima are associated with tropical convection over continents and the ITCZ as well as the Asian monsoon circulation in boreal summer (Fig. 11c), and maxima in the North Pacific as well in this season. Dry regions are seen in similar locations to AIRS data (Fig. 2), over the North Pacific and Asia in December–February (Fig. 11a) and west of the Asian monsoon region and the south Indian Ocean in June–August (Fig. 11c). The morphology of these regions appears slightly different in the model. For example, the dry region west of the Asian monsoon extends farther west.

High latitudes in the simulation are not as dry, as observed in Fig. 2, likely because the coarse vertical resolution of the model simulation does not resolve the lower stratosphere well. Gradients of RH are seen across the model tropopause. The Southern Hemisphere subtropics over the Indian Ocean (Fig. 11c) is nearly as dry as observations (Fig. 2c), but elsewhere the subtropics, and the equatorial eastern Pacific, appear moister. This is consistent with Fig. 10b. The moist subtropical bias is a known feature of general circulation models and analysis systems.

Model-simulated RH at 696 hPa is illustrated in Fig. 12. The ITCZ is a band of high humidity, with a branch

always in the Northern Hemisphere and a more pronounced double peaked meridional structure, particularly in December–March (especially in the eastern Pacific in Figs. 12a and 12b). This structure is much different than the observations (Figs. 3a and 3b). Convective maxima over continents are well reproduced. The wintertime subtropical minima (Figs. 12a and 12c) are as dry (if not drier) than AIRS observations (Figs. 3a and 3c), but the dry regions are smaller. On the whole, the patterns are fairly well represented.

For quantitative comparisons, we can also take the zonal mean AIRS RH data interpolated to CAM levels and subtract it from the zonal mean of the CAM simulation points with cloud fraction less than 70% for 2003. The zonal mean CAM RH and differences from AIRS for January and July are shown in Fig. 13. CAM RH is less than 30% in the subtropics, less than 20% in Southern Hemisphere winter (Fig. 13c), and AIRS is about 5%–10% drier (Fig. 13d), consistent with Fig. 10b. This difference is pretty constant throughout the year and maximizes in the lower troposphere near 600 hPa in middle latitudes (Figs. 13b,d), consistent with Fig. 10c. Differences in the Tropics are also seen at higher altitudes near 200 hPa, with AIRS up to 10%–15% drier at 250 hPa. This is not necessarily a model “bias,” but might simply be because AIRS has a lower effective threshold of cloud fraction for retrieval than assumed (i.e., there is closer correspondence between AIRS and CAM with cloud fractions less than 0.5). As an estimate of the sensitivity to clouds, simulated RH is 3% higher if the model output is not screened by cloud cover and it is drier if the screening is applied to even lower thresholds of cloud. The difference is similar to the expected dry bias noted by Soden and Fu (1995) comparing TOVS UTH with radiosondes.

Note that there are significant differences in the ex-

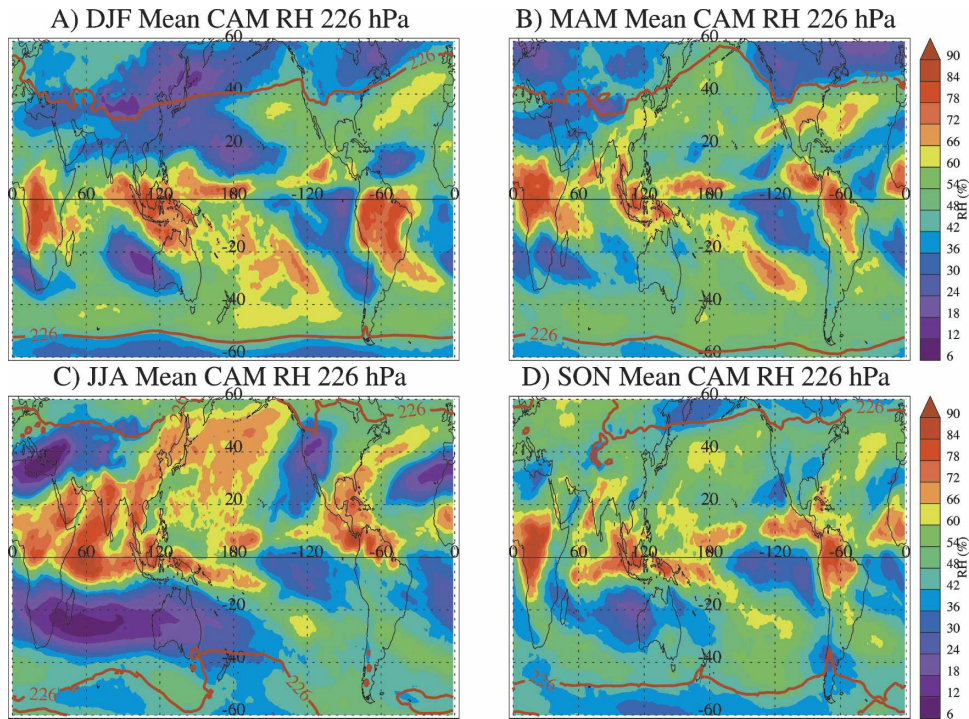


FIG. 11. Seasonal mean CAM relative humidity (%) at 226 hPa for (a) Dec–Feb, (b) Mar–May, (c) Jun–Aug, and (d) Sep–Nov. Thick red line is the seasonal tropopause at 226 hPa in the model.

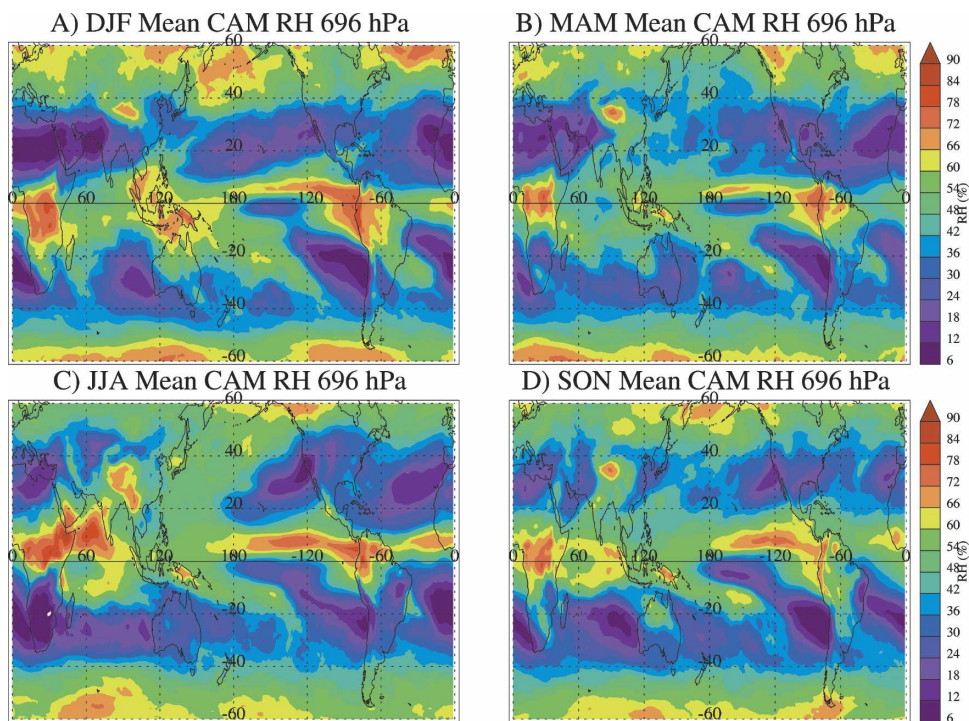


FIG. 12. Seasonal mean CAM relative humidity (%) at 696 hPa for (a) Dec–Feb, (b) Mar–May, (c) Jun–Aug, and (d) Sep–Nov.

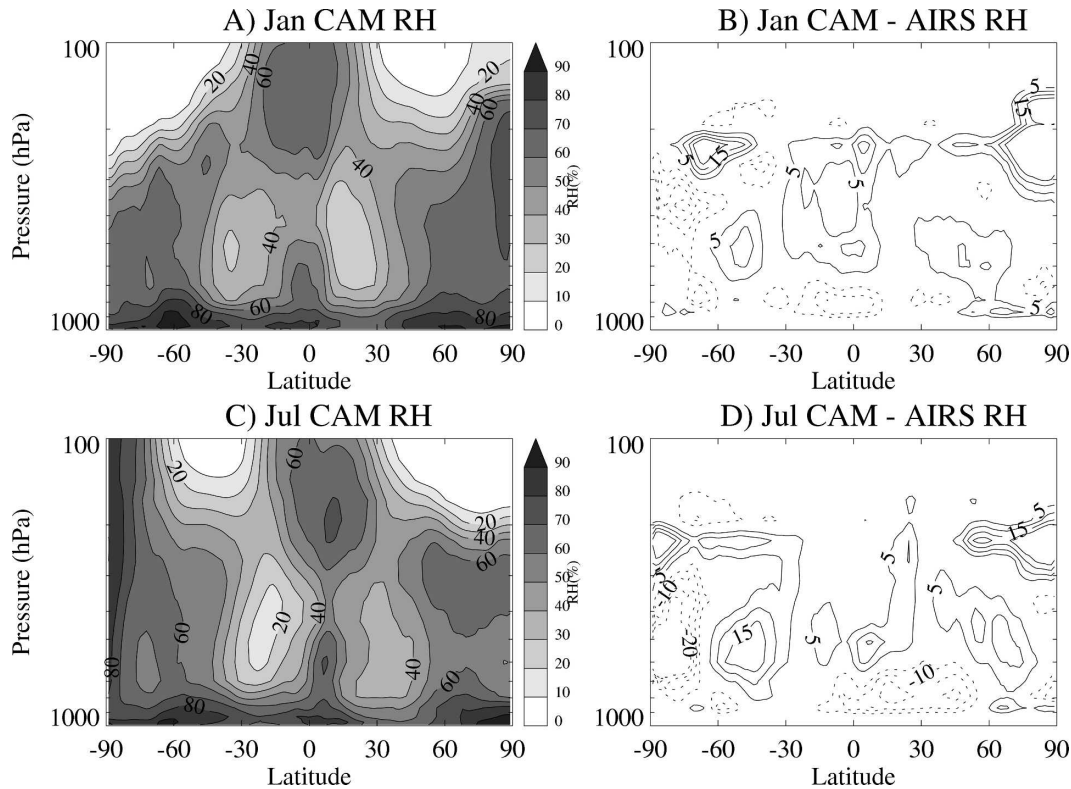


FIG. 13. Zonal mean RH (%) and differences as a function of latitude and height for (a) Jan mean CAM RH, (b) Jan difference (CAM – AIRS), (c) Jul mean CAM RH, and (d) Jul difference (CAM – AIRS).

tropical lower stratosphere in both hemispheres (at 250 hPa) and that the model is significantly drier than AIRS at low altitudes (below 600 hPa). Since we are focused on the upper troposphere, we will not discuss these differences at length. Differences at 250 hPa are in the stratosphere, where AIRS has trouble sensing water vapor and where the model does not have good resolution. We have not fully investigated lower troposphere and near-surface data from AIRS below 600 hPa, which may also be impacted by the surface treatment in the model.

b. Simulated variability

It is also instructive to examine not just seasonal means, but variability in the simulations. Figure 14 illustrates the daily standard deviation of upper-tropospheric RH from the model. The color scale is not the same as in Fig. 6. In general, variability in the model in midlatitudes is lower than the observations but still shows some maxima around the tropopause. Maxima are still visible in the North Pacific and to a lesser extent in the North Atlantic in winter (Fig. 14a). Maxima are also evident in the Southern Hemisphere midlatitudes into the South Pacific convergence zone in winter

(Fig. 14c) and low variability (coincident with low RH) in the subtropical Southern Hemisphere in this same season, at least over the Indian Ocean. Variability in general appears more scattered and not as directly tied to stratosphere–troposphere exchange, which is not well represented by the coarse vertical resolution of the model. Interestingly, the Tropics have higher variability than the observations, with slightly higher variability at the edge of the Tropics (10° – 15° off the equator) in most seasons, which is not seen in the observations.

This variability is seen in a Hovmöller plot of the simulated tropical mean daily RH at each longitude (Fig. 15). The data have been filtered to regions with high cloud fraction below 0.7. The model shows a stronger signal of continental convection over Africa and South America throughout the year than the observations (Fig. 9). The Asian monsoon circulation is smaller and farther west than the observations, and the humidity in the eastern Pacific stays low all year round up to the coast of South America, in contrast to the observations (Fig. 9). There is a signature of the Australasian monsoon at 120° E longitude from November to February, but there is also persistent high RH centered at 100° E longitude over Indonesia and the Malay penin-

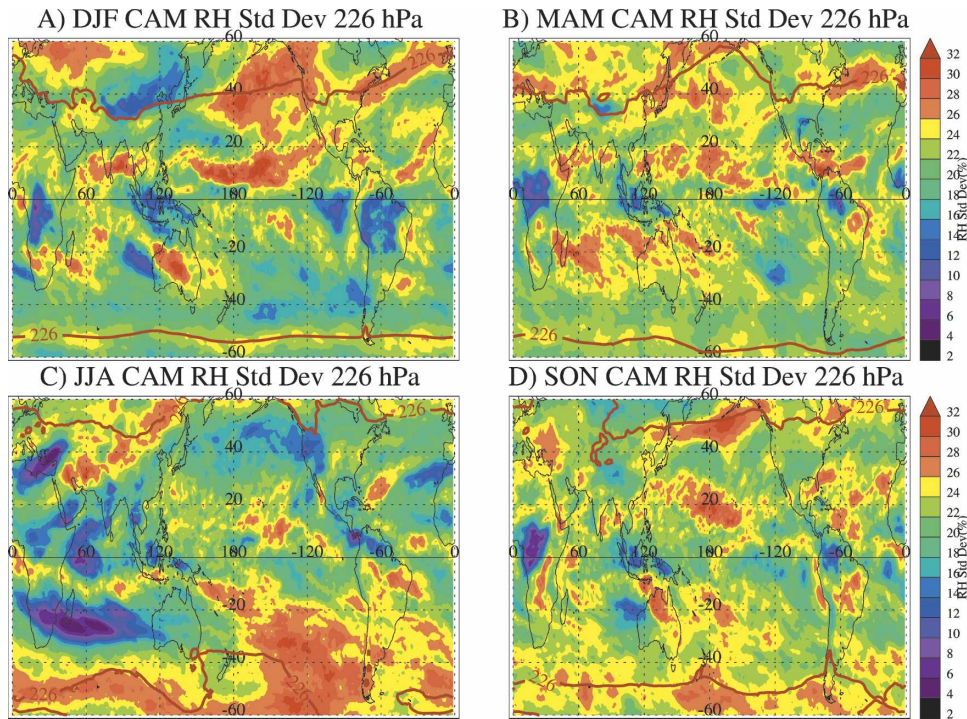


FIG. 14. As in Fig. 11 but for seasonal mean standard deviation of CAM relative humidity (%).

sula, which is not as noticeable in observations. There is no signature of the MJO in the simulations.

In other regions (the subtropics and the extratropics) the model is similar to the observations in Figs. 8 and 7.

In the subtropics the Asian monsoon is dominant, and both easterly and westerly waves can be seen, with some evidence of boreal winter intrusions. In the mid-latitudes the storm track dominates, but with less over-

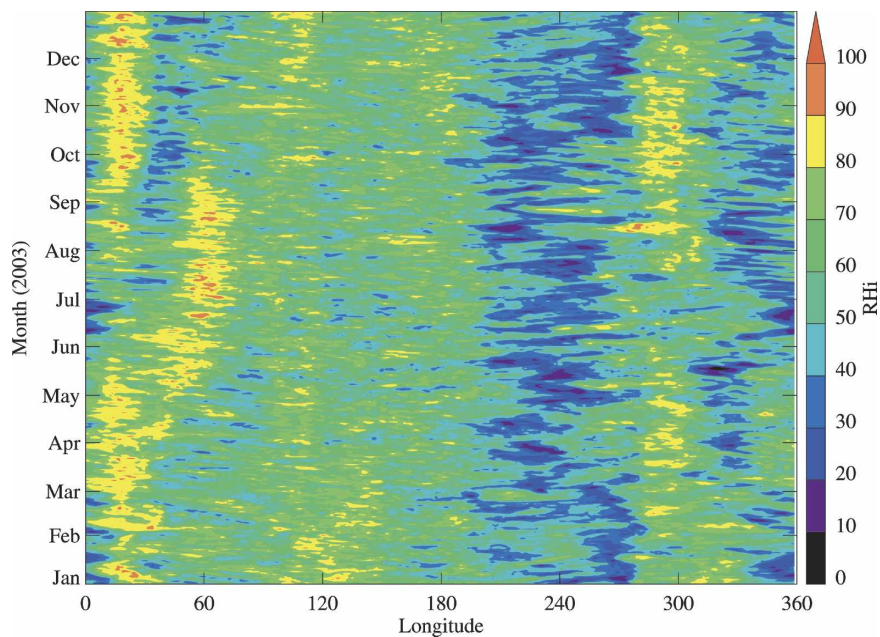


FIG. 15. Hovmöller plot of daily CAM relative humidity (%) at 226 hPa averaged over 10°S–10°N latitude.

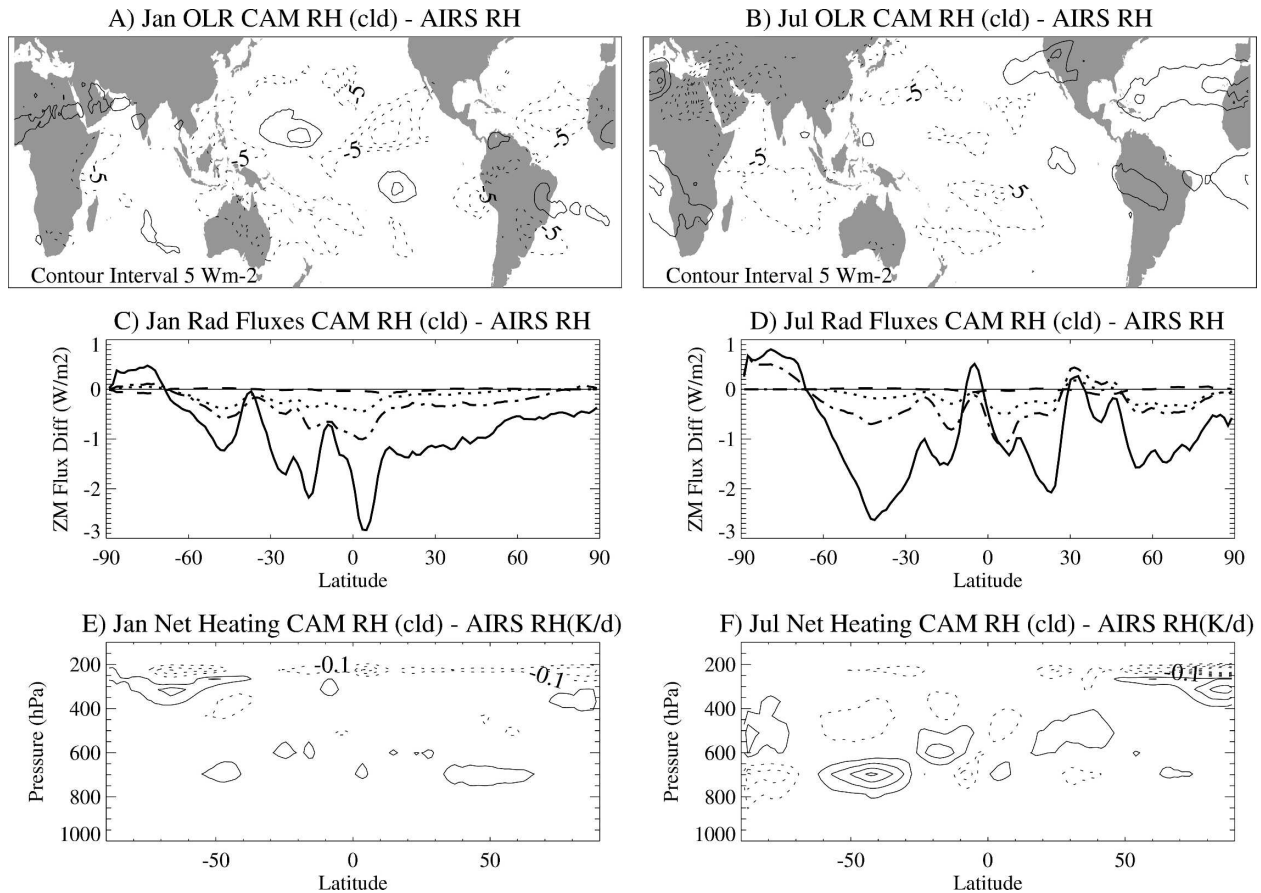


FIG. 16. Differences between CAM humidity sorted by cloud fraction (CAM) and AIRS humidity between 600 and 200 hPa (AIRS). Longwave radiation at the top of the atmosphere for (a) Jan and (b) Jul. Contour interval: 5 W m^{-2} . Zonal mean longwave radiation at the top (solid) and surface (dotted-dashed) and shortwave radiation at the top (dash) and surface (dotted) for (c) Jan and (d) Jul. Latitude height difference in net heating rate for (e) Jan and (f) Jul. Contour interval: $\pm 0.1 \text{ K day}^{-1}$.

all variability in the upper troposphere, partly due to the lack of appropriate gradients between the stratosphere and troposphere.

c. Impact on climate

Do the differences between the model and observations matter for climate? To answer this question we examine heating rates and radiative fluxes using an offline version of the CAM3 radiation code (Collins et al. 2002) for simulated RH and AIRS RH. We assume clear sky conditions because AIRS does not observe cloudy scenes. Simulated RH is derived from monthly means of the $1^\circ \times 1.25^\circ$ CAM simulation, sorted for all points with cloud fraction < 0.7 . For the AIRS RH case we replace the monthly mean simulated specific humidity between 600 and 200 hPa with AIRS humidity (done in relative humidity space so that $Q_{\text{AIRS}} = \text{RH}_{\text{AIRS}} / \text{RH}_{\text{CAM}} \times Q_{\text{CAM}}$).

Figure 16 illustrates the comparisons for January and

July between runs with CAM humidity sorted by cloud fraction (CAM) and AIRS humidity between 600 and 200 hPa (AIRS). The humidity changes are those of Fig. 13 between 600 and 200 hPa. Throughout most of this region, the model has higher relative humidity (Fig. 13) and, by the definition of this calculation, also more specific humidity (since the input temperatures are the same).

The resulting zonal mean top-of-atmosphere outgoing longwave radiation (OLR) differences are on the order of $1\text{--}3 \text{ W m}^{-2}$ (Figs. 16c and 16d) with a global mean of 1.1 W m^{-2} . Regional differences are as large as 15 W m^{-2} (Figs. 16a and 16b). The model, with higher humidity in the middle and upper troposphere, has lower OLR, indicating a warming of the atmosphere and lower radiation to space. An examination of total precipitable water associated with the humidity change indicates that the simulation has more precipitable water than AIRS RH. In general, the peaks occur in the

Tropics and subtropics (Figs. 16c and 16d), which might have a significant effect upon the radiative budget of the planet.

Heating rate profiles in Figs. 16e and 16f indicate the differences in net heating (longwave plus shortwave). The model has increased cooling in the upper troposphere and increased heating in the middle and lower troposphere. The difference in cooling in the subtropics reaches about 10% of the heating rate at 600–400 hPa and up to 30% in July at 50°S. This implies that the model has a clear sky tendency toward less stable conditions (heating below, cooling above), which is important for cloud formation. Differences in the extratropical lower stratosphere at 200 hPa are larger, but likely anomalous.

5. Discussion and conclusions

A relative humidity product has been derived from satellite retrievals of temperature and specific humidity from the AIRS sensor. Qualitatively AIRS RH validates well against in situ data, with a scatter relative to reference in situ sensors of ~ 10%–20% for levels at 250 hPa and below.

This work verifies that AIRS data reproduce major known features of the humidity distribution. These include high RH in the tropical troposphere and in the midlatitude upper troposphere and very low RH (as low as 10%) in the subtropics. The southeastern Pacific and South Atlantic Oceans are particularly dry regions. The seasonal cycle of humidity in the Tropics and subtropics follows the expected pattern of the Hadley–Walker circulation.

In addition, AIRS can provide significant new insight. This climatology is only a beginning. We highlight several important results in the data that deserve future study: (a) AIRS can discern the detailed vertical structure of humidity with a minimum in the middle troposphere and coupling between the upper and lower troposphere. (b) AIRS data provide a comprehensive look at daily and longer time scales of variability, including wave structures, and the complex humidity variations of the Asian summer monsoon circulation. (c) AIRS data are an important evaluation tool for climate models, a sample of which appears to perform well in general, but has trouble with variability and moist biases in the subtropics and in the vertical, which may change heating profiles.

a. Vertical structure

AIRS data are very useful for understanding the vertical structure of upper-tropospheric humidity. Many

regions appear to have a RH minimum in the middle troposphere, with moistening from the surface and a connection to moistening aloft through convection. The increase in RH in the upper troposphere appears to be at ~400 hPa, which corresponds to a temperature of ~240 K, near the level at which we expect ice processes to dominate. We expect higher RH in regions dominated by ice since ice processes have generally higher expected RH before crystal formation. The coupling in the vertical between the lower and upper troposphere can be clearly seen in convective regions where there is higher variability in the middle and upper troposphere, especially in the Tropics.

b. Temporal variability

AIRS can observe humidity changes associated with baroclinic storms, subtropical intrusions, and tropical cyclones. Signatures of the Madden–Julian oscillation are seen in the near-equatorial regions. Variability in humidity is largest in the winter extratropical storm track regions and conforms very closely to the tropopause in the upper troposphere. Variability is presumably driven by alternating moist tropospheric storms and dry stratospheric intrusions, and the climatology resembles the regions of warm conveyor belts and high troposphere–stratosphere exchange (Sprenger and Wernli 2003). In addition to dominant westerly waves, the Asian summer monsoon region also features easterly waves off the southern branch of the monsoon and appears clearly as a broad and sudden jump in lower-tropospheric humidity over India, extending up to 700 hPa.

Dry intrusions are seen in the subtropics, particularly in the Northern Hemisphere eastern Pacific in boreal winter and spring and over the Indian Ocean and Australia in winter and spring (June–November). The region to the west of the monsoon is also very dry, indicating that humidity does not mix isotropically out of the monsoon at upper levels. Premonsoon humidity at upper levels is also low, before moistening through convection. The dry regions with low water vapor are at the edge of AIRS sensitivity, and an examination of their dynamics is a subject for future study with other sensors.

Interannual variability cannot be discerned from the short record available from AIRS; however the annual cycle is repeatable, and variations appear to be less than the standard deviation of daily measurements. No strong forcings (e.g., ENSO events) are present in the data record. Over time, AIRS and subsequent instruments will provide a uniquely detailed look at these lower-frequency atmospheric oscillations.

c. Climate model comparisons

Comparisons to a climate model (CAM3) at similar resolution indicate that the model generally represents mean relative humidity well. The model is $\sim 6\%$ RH more moist than AIRS throughout much of the troposphere, even when sorted for significant cloudiness. Given that the bias also persists in clear regions, it is not an impact of cloud clearing. Biggest seasonal differences are due to the persistence of a double ITCZ in the Tropics. Some of the differences may be due to model difficulties in representing the vertical transport of humidity, and too much moistening of the air above the boundary layer. Vertical profile comparisons indicate that the model has much larger midtropospheric humidity in the Tropics and in midlatitudes.

Variability in the model and particularly in the Tropics and subtropics is not as well simulated as the mean and seasonal cycle. This is a general feature of GCMs and is not a problem with representations of RH per se, but rather a general issue with the representation and initiation of convection. Differences in the Tropics and subtropics result in zonal mean differences in heating rates of $\sim 10\%$ in the upper troposphere and zonal mean OLR differences of $1\text{--}3\text{ W m}^{-2}$, with a global average near 1 W m^{-2} . In some regions, such as the extremely dry upper troposphere west of the Asian monsoon, differences are up to 15 W m^{-2} .

These differences may have important impacts for climate variability and climate change simulations in the Tropics. For example, less radiation to space in the subtropics might tend to damp the subsidence cooling and correspondingly reduce the strength of the Hadley circulation. Differences in the vertical heating structure may affect atmospheric stability and clouds. However, these changes are idealized (clear sky), and basically diagnostic, reflecting properties of a tightly coupled interaction between radiation and cloud processes in the model. Nonetheless, it is a useful diagnostic test for climate simulations. Continued improvements to the hydrologic cycle and representation of deep convective activity are critical areas for representing climate and climate variability properly. AIRS observations provide a detailed and quantitative picture for model comparisons and for more detailed process studies of clouds, temperatures, and humidity.

d. Future prospects

Critical to the long-term value of AIRS for climate will be the stability and a long time series of measurements. For climate prediction, AIRS measurements need to be stable and maintained over a long period of time. Similar measurements to AIRS will be taken from

the future National Polar-Orbiting Operational Environmental Satellite System (NPOESS) platforms by the Cross Track Infrared and Advanced Technology Microwave Sounder (CrIMSS) sensor suite. The climate community needs to make certain that the capabilities of AIRS on *Aqua* transfer to CrIMSS on NPOESS so that we have a continuous record of quality climate-calibrated humidity measurements over the next 20 years.

Acknowledgments. We thank William Randel, Mijeong Park, and three anonymous reviewers for comments. This research at the National Center for Atmospheric Research (NCAR) was supported by NASA Grant EOS/03-0594-0572.

REFERENCES

- Aumann, H. H., and Coauthors, 2003: AIRS/AMSU/HSB on the *Aqua* mission: Design, science objectives, data products, and processing systems. *IEEE Trans. Geosci. Remote Sens.*, **41**, 253–264.
- Bates, J. J., and D. L. Jackson, 2001: Trends in upper-tropospheric humidity. *Geophys. Res. Lett.*, **28**, 1695–1698.
- Collins, W. D., J. K. Hackney, and D. P. Edwards, 2002: An updated parameterization for infrared emission and absorption by water vapor in the National Center for Atmospheric Research Community Atmosphere Model. *J. Geophys. Res.*, **107**, 4664, doi:10.1029/2001JD001365.
- , and Coauthors, 2006: The formulation and atmospheric simulation of the Community Atmosphere Model Version 3 (CAM3). *J. Climate*, **19**, 2122–2143.
- Divakarla, M. G., C. D. Barnett, M. D. Goldberg, L. M. McMillin, E. Maddy, W. Wolf, L. Zhou, and X. Liu, 2006: Validation of Atmospheric Infrared Sounder temperature and water vapor retrievals with matched radiosonde measurements and forecasts. *J. Geophys. Res.*, **111**, D09S15, doi:10.1029/2005JD006116.
- Eckhardt, S., A. Stohl, H. Wernli, P. James, C. Forster, and N. Spichtinger, 2004: A 15-year climatology of warm conveyor belts. *J. Climate*, **17**, 218–237.
- Eguchi, N., and M. Shiotani, 2004: Intraseasonal variations of water vapor and cirrus clouds in the tropical upper troposphere. *J. Geophys. Res.*, **109**, D12106, doi:10.1029/2003JD004314.
- Elliot, W. P., and D. J. Gaffen, 1991: On the utility of radiosonde humidity for climate studies. *Bull. Amer. Meteor. Soc.*, **72**, 1507–1520.
- Fetzer, E., and Coauthors, 2003: AIRS/AMSU/HSB validation. *IEEE Trans. Geosci. Remote Sens.*, **41**, 418–431.
- Gettelman, A., and Coauthors, 2004: Validation of *Aqua* satellite data in the upper troposphere and lower stratosphere with in situ aircraft instruments. *Geophys. Res. Lett.*, **109**, L22107, doi:10.1029/2004GL020730.
- , E. J. Fetzer, A. Eldering, and F. W. Irion, 2006a: The global distribution of supersaturation in the upper troposphere from the Atmospheric Infrared Sounder. *J. Climate*, **19**, 6089–6103.
- , V. P. Walden, L. M. Miloshevich, W. L. Roth, and B. Halter, 2006b: Relative humidity over Antarctica from radiosondes, satellites, and a general circulation model. *J. Geophys. Res.*, **111**, D09S13, doi:10.1029/2005JD006636.
- Goff, J. A., and S. Gratch, 1946: Low-pressure properties of water

- from -160°F to 212°F . *Trans. Amer. Soc. Heat. Vent. Eng.*, **52**, 95–121.
- Hartmann, D. L., and K. Larson, 2002: An important constraint on tropical cloud–climate feedback. *Geophys. Res. Lett.*, **29**, 1951, doi:10.1029/2002GL015835.
- , and M. L. Michelsen, 2002: No evidence for iris. *Bull. Amer. Meteor. Soc.*, **83**, 249–254.
- Jackson, D. L., and J. J. Bates, 2001: Upper tropospheric humidity algorithm assessment. *J. Geophys. Res.*, **106**, 32 259–32 270.
- Jensen, E. J., and Coauthors, 2000: Prevalence of ice supersaturated regions in the upper troposphere: Implications for optically thin ice cloud formation. *J. Geophys. Res.*, **106**, 17 253–17 266.
- Miloshevich, L. M., H. Vömel, D. N. Whiteman, B. M. Lesht, F. J. Schmidlin, and F. Russo, 2006: Absolute accuracy of water vapor measurements from six operational radiosonde types launched during AWEX-G, and implications for AIRS validation. *J. Geophys. Res.*, **111**, D09S10, doi:10.1029/2005JD006083.
- Mote, P. W., H. L. Clark, T. J. Dunkerton, R. S. Harwood, and H. C. Pumphrey, 2000: Intraseasonal variations of water vapor in the tropical upper troposphere and tropopause region. *J. Geophys. Res.*, **105**, 17 457–17 470.
- Murphy, D. M., and T. Koop, 2005: Review of the vapour pressure of ice and supercooled water for atmospheric applications. *Quart. J. Roy. Meteor. Soc.*, **131**, 1539–1565.
- Randel, W. J., and M. Park, 2006: Deep convective influence on the Asian summer monsoon anticyclone and associated tracer variability observed with Atmospheric Infrared Sounder (AIRS). *J. Geophys. Res.*, **111**, D12314, doi:10.1029/2005JD006490.
- Read, W. G., J. W. Waters, D. A. Flower, L. Froidevaux, R. F. Jarnot, D. L. Hartmann, R. S. Harwood, and R. B. Rood, 1995: Upper tropospheric water vapor from UARS MLS. *Bull. Amer. Meteor. Soc.*, **76**, 2381–2389.
- , and Coauthors, 2001: UARS microwave limb sounder upper tropospheric humidity measurement: Method and validation. *J. Geophys. Res.*, **106**, 32 207–32 258.
- Rind, D., E. W. Chiou, W. Chu, S. Oltmans, J. Lerner, J. Larson, M. P. McCormick, and L. McMaster, 1993: Overview of the stratospheric aerosol and gas experiment ii water vapor observations: Method, validation, and data characteristics. *J. Geophys. Res.*, **98**, 4835–4856.
- Soden, B. J., and F. P. Bretherton, 1994: Evaluation of water vapor distribution in general circulation models using satellite observations. *J. Geophys. Res.*, **99**, 1187–1210.
- , and R. Fu, 1995: A satellite analysis of deep convection, upper-tropospheric humidity, and the greenhouse effect. *J. Climate*, **8**, 2333–2350.
- , and J. R. Lazante, 1996: An assessment of satellite and radiosonde climatologies of upper-tropospheric water vapor. *J. Climate*, **9**, 1235–1250.
- Sprenger, M., and H. Wernli, 2003: A northern hemispheric climatology of cross-tropopause exchange for the ERA15 time period (1979–1993). *J. Geophys. Res.*, **108**, 8521, doi:10.1029/2002JD002636.
- Susskind, J., C. D. Barnett, and J. M. Blaisdell, 2003: Retrieval of atmospheric and surface parameters from AIRS/AMSU/HSB data in the presence of clouds. *IEEE Trans. Remote Sens.*, **41**, 390–409.
- Tobin, D. C., and Coauthors, 2006: Atmospheric Radiation Measurement site atmospheric state best estimates for Atmospheric Infrared Sounder temperature and water vapor retrieval validation. *J. Geophys. Res.*, **111**, D09S14, doi:10.1029/2005JD006103.
- Udelhofen, P. M., and D. L. Hartmann, 1995: Influence of tropical cloud systems on the relative humidity of the upper troposphere. *J. Geophys. Res.*, **100**, 7423–7440.
- Waugh, D. W., 2005: Impact of potential vorticity intrusions on subtropical upper tropospheric humidity. *J. Geophys. Res.*, **110**, D11305, doi:10.1029/2004JD005664.